QUARTERLY JOURNAL OF THE ROYAL METEOROLOGICAL SOCIETY
Q. J. R. Meteorol. Soc. **134**: 841–857 (2008)
Published online 27 May 2008 in Wiley InterScience
(www.interscience.wiley.com) DOI: 10.1002/qj.260

RMetS
ROYAL METEOROLOGICAL SOCIETY

The life cycle of convective-shower cells under post-frontal conditions

Tanja Weusthoff* and Thomas Hauf
Institute of Meteorology and Climatology, Leibniz Universität Hannover, Germany

ABSTRACT: Seventeen days with post-frontal shower precipitation are analysed by means of radar data obtained from the German Weather Service's C-band radar network. The life cycle of clusters – defined here as contiguous rain areas including one or more radar-reflectivity peaks (i.e. convection cells) – is investigated. To allow for the continuous tracking of clusters, sometimes over a time period of more than an hour, a new, specially adapted tracking algorithm has been developed. The life cycle of convective clusters comprises five different stages: genesis; growth (including merging); stagnation; decay (including splitting); and dissolving. The transition likelihoods from a cluster with n maxima to one with m maxima are determined (the case $m > n$ corresponding to growth and $m < n$ to decay). It is found that, predominantly, clusters grow or decay by one cell. Results relating to the temporal evolution of post-frontal showers are presented, and a conceptual growth model is proposed. Although single cells are the most frequent cluster type, the spatial structure of the post-frontal precipitation field is dominated by multi-celled clusters. Their life cycle is essentially affected by cell merging and splitting. Although the transitions of all (about one million) identified clusters have been analysed and quantified, more research is necessary in order to understand the underlying principles of cluster growth. Copyright © 2008 Royal Meteorological Society

KEY WORDS convection; precipitation; radar; tracking

Received 15 August 2007; Revised 19 February 2008; Accepted 14 April 2008

1. Introduction

1.1. General

Under post-frontal conditions, i.e. in the cold air mass behind a cold front, areas of several tens of thousands of square kilometres with shower precipitation can often be found. The satellite image in Figure 1 shows an example of the corresponding convective clouds. At first glance, post-frontal showers do not exhibit a uniform structure, but reveal an apparently irregular distribution. Previous studies by Theusner (2007) and Theusner and Hauf (2004) showed that the spatial structure of precipitating shower clouds, as measured by the C-band radar network of the German Weather Service (DWD), follows simple analytical equations and distributions. The latter refer to the number of contiguous precipitating shower clouds, their size, the number of individual cells of which they are composed, the distances between those cells, and the diurnal cycle of these parameters. Theusner (2007) essentially found a log-normal distribution for the size of clusters with a given cell number, as well as a power law for the frequency distribution of clusters with different cell numbers (see Section 4).

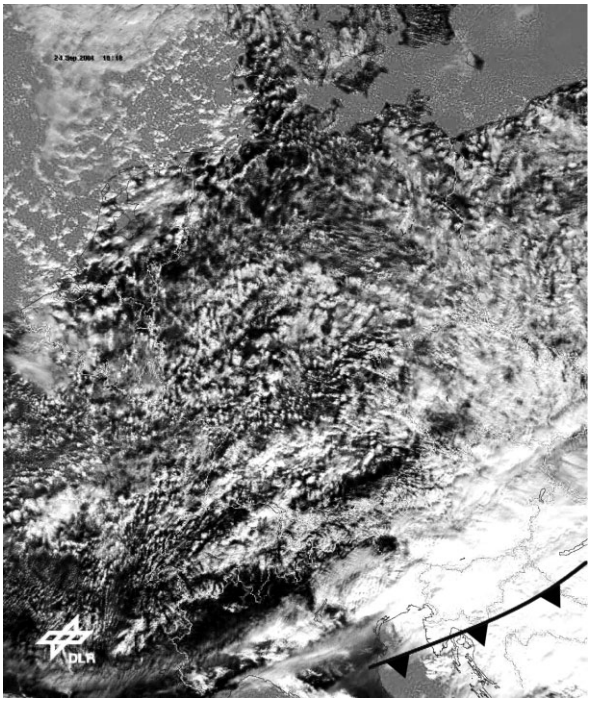

Figure 1. Post-frontal shower clouds over central Europe (NOAA, AVHRR, visible channel; 24 September 2004, 1018 UTC). Source: DLR.

In this paper, we expand that work, and analyse the life cycle of shower clouds by tracking them individually over time. The main objective is to identify and describe the various stages of the life cycle and the interactions

* Correspondence to: Tanja Weusthoff, Institute of Meteorology and Climatology, Leibniz Universität Hannover, 30419 Hannover, Germany. E-mail: weusthoff@muk.uni-hannover.de

between different clusters. Subsequent work will focus on the amount of rain a cluster produces and, finally, on the quantitative description of the temporal development.

Theusner (2007) performed an Eulerian-type analysis at fixed times, 15 min apart. Here, we use a new radar product with a time separation of only 5 min, and perform a Lagrangian-type analysis. The ultimate objective is to combine both sets of results for a hybrid shower-forecasting system; this is done in the context of the priority programme 1167 'Quantitative Precipitation Forecast' of the German Research Foundation. The term 'hybrid' refers to the fact that the post-frontal area is forecast conventionally by numerical weather-prediction models while the shower structure itself is described statistically.

1.2. Tracking and cell development

Precise tracking of clouds is a key requirement in many remote-sensing applications. Existing tracking algorithms for clouds or cloud systems were mainly developed for deep convective systems, primarily for purposes of monitoring, nowcasting and warning. Examples of such algorithms include KONRAD in Germany (Lang *et al*., 2003), GANDOLF in the United Kingdom (Pierce *et al*., 2000), and TITAN (Dixon and Wiener, 1993) and TREC (Rinehart and Garvey, 1978) in Colorado. Wilson *et al*. (1998) and Dixon and Wiener (1993) give a broad overview of various methods of storm tracking and nowcasting using radar, satellite or lightning data. Some of these methods use two-dimensional data fields for pattern recognition (Austin, 1985) or cross-correlation techniques (Rinehart, 1981; Tuttle and Foote, 1990); others consider three-dimensional storm entities, for example to perform so-called centroid tracking (Austin and Bellon, 1982; Witt and Johnson, 1993). Within the World Weather Research Programme Forecast Demonstration Project ('Sydney 2000'), Pierce *et al*. (2004) performed a statistical and study-oriented comparison of four different radar-based nowcasting schemes. They found centroid tracking and pattern-matching extrapolation techniques to be most reliable in convective scenarios. Whereas older techniques use a simple extrapolation to determine the new object position (e.g. Dixon and Wiener, 1993; Johnson *et al*., 1998), more recent techniques also forecast storm initiation, growth and dissipation (e.g. Mueller *et al*., 2003; Pierce *et al*., 2000). Some of these studies also deal with the life cycle, and with the interactions of cells, such as merging or splitting, which are critical in life-cycle determination (Li and Lai, 2004; Carvalho and Jones, 2001).

The initiation and development of convective clouds is not fully understood, and is a topic of ongoing research. The common idea of the life cycle of a single thunderstorm goes back to the early model proposed by Byers and Braham (Braham, 1996) following the Thunderstorm Project in the late 1940s. They defined three stages in the life of a thunderstorm: a towering-cumulus stage, a mature stage, and a dissipating stage (Bluestein, 1993). They also recognized the formation of individual cells in clusters. Although not explicitly dealt with at that time, it was later shown that this implies interactions among individual cells that may have consequences for the convective evolution (e.g. Jewett and Wilhelmson, 2006).

Bluestein (1999) gives a historical overview of field programmes dedicated to the study of severe convective storms. With the help of such field measurements and numerical modelling, the internal structure and evolution of convective clouds and cloud systems have been investigated over the past fifty years.

Merging (the combining of two or more convective systems), as an important element of the growth of convective-cloud systems, was the subject of a number of studies in the 1970s and 1980s (Westcott, 1984). Merging cells were found to grow larger, and produce more precipitation, than isolated cells. Numerical case studies focused on the merging process itself and the factors controlling it. Among the contributing factors identified were: a favourable pressure gradient (Turpeinen, 1982); low-level convergence (Tao and Simpson, 1989); a new cell bridging existing cells; and differential cell motion (Cunning *et al*., 1982; Westcott and Kennedy, 1989). In a case study including two convective periods, Westcott (1994) found that horizontal expansion was the main reason for cells merging. Only in 15% of cases did differential motion or the growth of a new cell core play an obvious role in causing cells to join. Recent studies have dealt with the effect of merging on supercells and squall lines or mesoscale convective systems with heavy precipitation (e.g. Lee *et al*., 2006a, 2006b; Fu and Guo, 2006).

Compared to the phenomenon of merging, the splitting of thunderstorms has been addressed by fewer studies. Splitting often occurs as a marginal phenomenon within field studies or simulations, but does not receive as much attention as merging processes. Bluestein *et al*. (1990) documented the initiation and behaviour of splitting convective clouds, and attributed this splitting to dynamic forcing effects rather than to rainwater loading. Jewett and Wilhelmson (2006) have investigated the role of splitting cells within squall lines using numerical simulations.

Almost all current research concerning tracking and nowcasting is related to thunderstorms. So far, to our knowledge, nothing similar has been done with regard to shower precipitation without lightning occurrence, i.e. showers mainly related to mid-level convection. For the purpose of investigating the development of showers in a post-frontal synoptic environment, a tracking algorithm that allows for an analysis of the processes involved is needed. Therefore we have developed a new tracking algorithm, which is described in Section 3.

1.3. Objectives

The formation of post-frontal showers is, to a certain degree, chaotic. It is difficult to predict when and where a

DOI: 10.1002/qj

rain-cloud will emerge and how it will develop – whether it will stay alone or attach itself to other clouds to form a larger complex. Rain duration within the precipitation field is shorter, and individual rain areas are smaller and have lower radar reflectivities (for example, in TITAN the minimum reflectivity was 35 dBZ (Dixon and Wiener, 1993), whereas in our case it is 20 dBZ); but these areas are more numerous than for deep convective cells. Thus, the complexity of the growth process, which is well recognized for deep convective cells, is even greater in the case of post-frontal showers.

We have investigated the development of convective-rain areas (also referred to as 'clusters') with the help of a newly-developed tracking algorithm. A cluster appears in a radar picture as a contiguous rain area with one or more enclosed maxima of radar reflectivity, or equivalently, of precipitation rate. Each maximum is assumed to represent a single convection cell. Figure 2 shows some examples of clusters with various sizes and shapes. The new algorithm allows tracking of individual clusters at time steps of 5 min, and thus investigation of their temporal development. The individual radar-reflectivity maxima, however, could not be tracked. Their number was determined at each time step simply by counting. For the present study, 17 days with post-frontal shower precipitation were investigated, with a total of more than one million individual rain areas.

In this paper we investigate the various processes constituting the life cycle of individual clusters: the genesis of a cluster; its changes over a specific time step (here 5 min); and finally its disappearance. As stated above, the classical view of shower growth refers to single cells growing horizontally (in area) and vertically, accompanied by intensifying precipitation rates. Radar observations, however, reveal a more complicated structure. Figure 3 illustrates this fact with a sequence of 5 min radar data. The individual cells combine into larger clusters and interact with each other in many different ways, resulting in a much more complicated life cycle than that assumed for pure single-cell growth.

Five different life stages can be identified immediately by visual inspection:

1. genesis;
2. growth (internal growth and merging);
3. stagnation;
4. decay (internal decrease and splitting);
5. dissolving.

Figure 2. Illustration of clusters of various sizes and shapes. Darker pixels correspond to lower radar reflectivity. The local maxima of a cluster are indicated by the white pixels inside the rain area. The single cell (left) has an areal extent of 105 km^2. The areas of the clusters on the right range from 700 km^2 (with 17 maxima) to 40 km^2 (single cell).

Figure 3. Development of various clusters over 15 min, illustrated with a sequence of radar data, with time in UTC. Clusters in all stages can be found in this sequence; they are illustrated in more detail in Figure 4.

These processes are illustrated in Figure 4. 'Genesis' means that the cluster appears for the first time in the radar data. 'Growth' is defined as an increase in the number of cells inside a cluster, either by internal growth or by merging with another cluster. 'Decay' refers to a decrease in the number of cells inside a cluster, either by internal decrease or by splitting into smaller clusters. 'Stagnation' means that the cluster does not change its size (in terms of the number of cells included). 'Dissolving' means the disappearance of a cluster within one time step.

A major difference between previous work and our study is that we investigate cluster growth with respect to the number of cells included. The temporal development of a cluster can generally be classified into two different types of growth and decay processes: one type is related to an areal increase or decrease of the cluster; the other to an increase or decrease in the number of constituting cells, or equivalently the number of precipitation-rate maxima contained in it. In this study we focus on the latter type of growth; areal growth will be the subject of a follow-up study. In this respect we follow the approach of Mesnard and Sauvageot (2003) and Theusner (2007), who investigated the structural characteristics of precipitation fields in relation to the cell number of the individual rain areas. Mesnard and Sauvageot (2003) used radar data from four single radars for their investigations (two stations located in France and two in the African Tropics), but did not distinguish between convective- and stratiform-rain events. Theusner (2007) used the national radar composite of the DWD, consisting of 16 radar stations, and thus covering a much larger area. He concentrated his analysis on post-frontal convective precipitation fields, which are also the subject of the present study.

The data used for our analysis are introduced in Section 2. In Section 3 the tracking algorithm is described. In Section 4, we present the findings of our study, which are then discussed in Section 5. A simple growth model is suggested to summarize the results.

2. Data

For the present analysis, a new radar product of the DWD national radar network, the RZ-composite, is used.

DOI: 10.1002/qj

The national radar network (*Radarverbund*) comprises 16 C-band radar stations with a spatial resolution of 1 km × 1 km. The RZ-composite is based on the so-called 'precipitation scan', whereby the atmosphere is scanned every 5 min, with an elevation angle ranging from 0.5° to 1.8°, depending on the local orography. As Figure 5 shows, the RZ-composite covers Germany and parts of the surrounding countries, a total of 557 304 km^2, equivalent to about 700 km × 800 km. For the RZ-composite, measured radar reflectivities (the so-called DX-product) are corrected for shadowing effects and converted into precipitation rates using an advanced $Z-R$ relationship (Weigl *et al.*, 2004), which distinguishes between stratiform and convective precipitation. The precipitation rate is accurate to within 0.01 mm per 5 min, or 0.12 mm h^{-1}. Data are received without a geographical underlay, which might otherwise distort the pixel-oriented data processing.

Following Theusner and Hauf (2004), the post-frontal area with a typical convective-precipitation field is identified using a semi-objective method. First, days with post-frontal showers are selected by visual inspection of satellite images in combination with 500 hPa and surface-weather charts. In this way, 17 days in 2004 and 2006, listed in Table I, are selected. For each day, the area with post-frontal precipitation is segmented semi-automatically by drawing a polygon around it. The segmented data are then stored for further processing. An example is shown in Figure 6. This selection process is to some extent subjective, and the future development of an automated algorithm is desirable.

To distinguish active shower cells from dynamically inactive or erroneous ones, it is necessary to define a threshold of either radar reflectivity or precipitation rate. The threshold precipitation rate used for this purpose

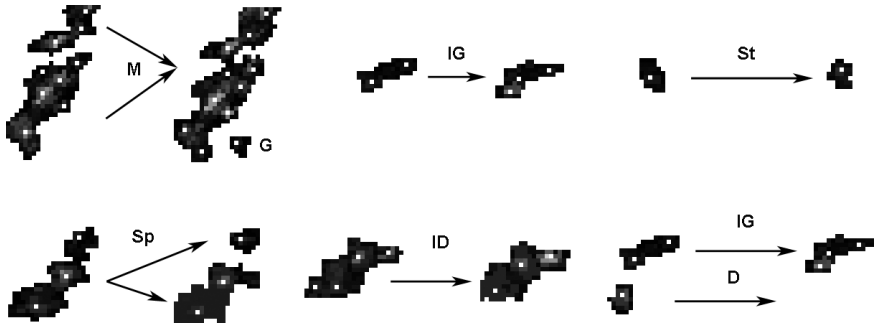

Figure 4. Illustration of processes in cluster development, extracted from the radar sequence in Figure 3. ('G' – genesis; 'M' – merging; 'IG' – internal growth; 'St' – stagnation; 'Sp' – splitting; 'ID' – internal decrease; 'D' – dissolving.)

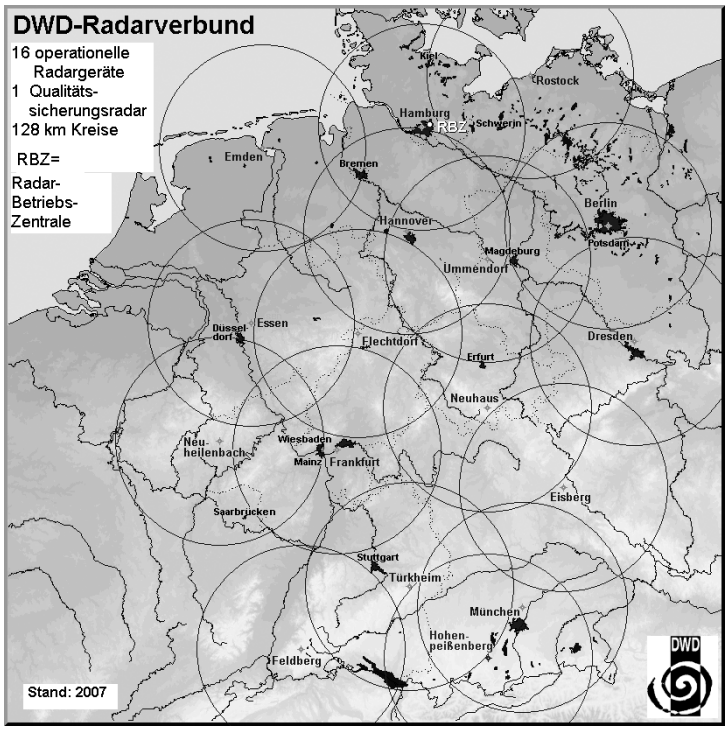

Figure 5. The German Weather Service national radar network (*Radarverbund*). The radius of the circles is 128 km. Source: DWD.

DOI: 10.1002/qj

Table I. List of days used for the analysis.

Year	Month	Dates
2004	February	25
	March	21
	May	23
	June	12
	July	10, 12
	August	13, 26, 31
	September	24
2006	January	21
	March	1, 2, 5, 6, 7
	November	9

is 0.05 mm per 5 min, or 0.6 mm h^{-1}, which corresponds to 20 dBZ. Theusner (2007) found this value to be sufficient for the unambiguous detection of convection cells. He also found that reducing the threshold did not increase the number of rain areas, while increasing it lowered the number of detected rain areas. Thus, for the sake of simplicity, in the present analysis we will only discuss results found with this threshold value.

For the identification of the individual convection cells inside the clusters, the radar images are first smoothed with a Gaussian filter, and then any pixel having a precipitation rate larger than that of all its eight neighbours is identified as a maximum. Mesnard and Sauvageot (2003) used a similar approach except that the neighbouring pixels had to be exceeded by a certain minimum amount in order for a pixel to be defined as a maximum. Theusner (2007) used radar images that only showed six steps of radar reflectivity (implying a threshold depending on the degree of image smoothing); the RZ product used in the present study has a much higher resolution (0.01 mm per 5 min). Our estimate of the number of cells is greater than that of those two studies. However, a recalculation of some of the structural investigations, such as the cell number distribution, with the RZ-composite yields results comparable to those of Theusner (2007). A sensitivity study for the cell-detection procedure is planned for subsequent analyses.

Altogether, we have identified an average of about 68 000 individual clusters per day, ranging from 30 000 to 119 000. The number of individual cells ranges from 63 000 to 268 000, with an average value of 154 000. Thus, on average, a cluster contains approximately two cells. The mean precipitation area ranges from 9000 km^2 to 30 000 km^2. Investigation of the precipitation area is left for further studies.

3. Tracking procedure

Investigation of a cluster over its life cycle requires tracking it from its genesis to its final decay. The tracking algorithm used in this study was developed by Weusthoff (2005), and is based on the DWD's 5 min RZ-composite. This algorithm combines various methods adapted from other tracking algorithms (see, for example, Section 1.2), such as correlation analysis and individual tracking.

Tracking is done in a five-step procedure (see Figure 7).

1. Every hour, the displacement vector of the whole precipitation field is determined by a correlation analysis using the newest data and those of 10 min earlier. For this part of the analysis, the threshold value applied to the radar image (see Section 2) is reset to zero. A single displacement vector for the whole precipitation field is derived: the small-scale structure of the wind field is not considered in this step.
2. At start time t_0, all contiguous rain areas within the radar image are identified and labelled (as illustrated in Figure 8). Various characteristics of each cluster are determined, such as:
   - the number of precipitation-rate maxima within the cluster (note that each maximum is considered as representing an individual convection cell);
   - the area;

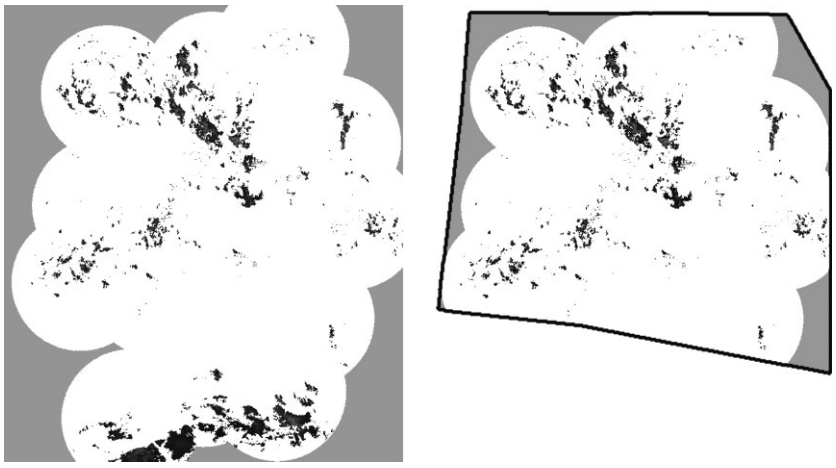

Figure 6. Selection of the post-frontal shower area: RZ-composite for 24 September 2004, 0210 UTC, with the coverage of the German radar network shown in white (left). The selected shower area is inside a polygon that is manually defined and drawn (right).

DOI: 10.1002/qj

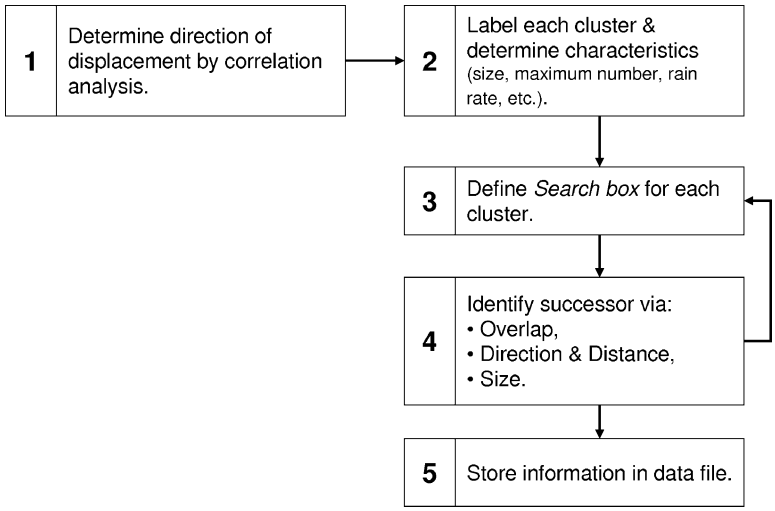

Figure 7. The tracking algorithm. See text for more details.

- the total amount of precipitation in the corresponding 5 min interval;
- the maximum precipitation rate observed at a pixel (1 km × 1 km) within the cluster area;
- the central coordinates of the cluster's encompassing ellipse.

3. To reidentify a cluster after 5 min, a 'search box' that encloses the actual cluster at start time t_0 is defined. Figure 9 shows how the size and position of this box are determined. The coordinates of the box edges are $(x_{\min} - \delta x, y_{\min} - \delta x)$ and $(x_{\max} + \delta x, y_{\max} + \delta x)$ where $x_{\min}$, $y_{\min}$, $x_{\max}$ and $y_{\max}$ are the minimum and maximum x and y values of the actual cluster. The parameter δx is set to a fixed value of 10 km. This means that we are searching a distance of 10 km in each direction, which is more than the maximum values generally found for the overall movement within a time step. This search box is applied to the radar image for the next time step. All clusters inside this box that are found within the new radar image at $t_0 + 5$ min are potential successors of the actual cluster (see Figure 9, left).
4. The most likely successor is identified from:
   - the amount of overlap (pixels covered by the same cluster at successive times) – for low propagation speeds, this overlap is large;
   - the difference in direction between the propagation of each potential successor and the overall movement (obtained by a correlation analysis of two successive radar pictures 10 min apart once every hour, as performed in step 1);
   - the distance between the actual cluster and the potential successor, determined by the distance between the coordinates of the encompassing ellipses' focal points (see step 2);
   - the difference between the sizes of the actual cluster and the potential successor.

   For details concerning the criteria, see Appendix B. Figure 9 shows an example of a successor identified through these criteria. The searching procedure is repeated for every time step from 0000 UTC to 2350 UTC, as long as data are available.
5. The cluster characteristics (such as size, cell number, and position), as well as the precursors and successors, are stored for further analysis (an example of such a parameter list is given in Appendix A). If more than one successor is found, they are all stored as successors of the initial cluster. If none are found, a termination mark is written in the parameter list. Knowing the precursor and successor of a cluster, we can investigate its growth and interactions with neighbouring clusters, and thereby relate its development to the number of cells it contains.

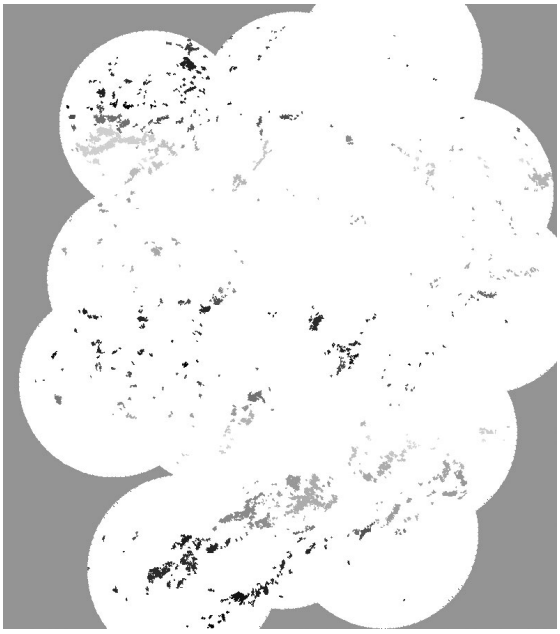

Figure 8. Illustration of cluster analysis: identification of contiguous rain areas or clusters. Identified and subsequently labelled clusters are represented by distinct shades of grey.

As stated in Section 1.2, interactions among clusters, such as splitting and merging, are critical for the tracking

DOI: 10.1002/qj

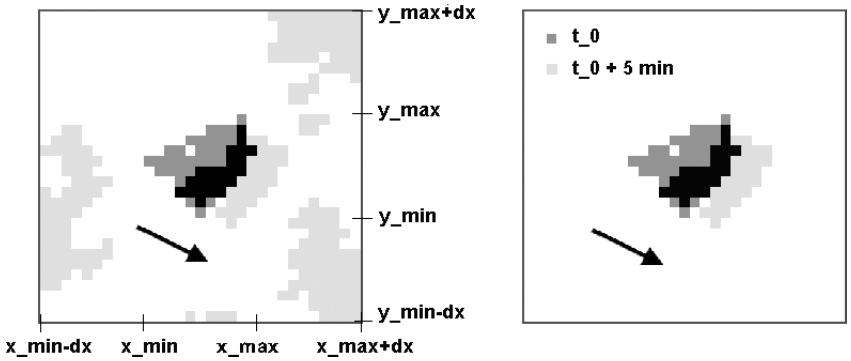

Figure 9. Example of a search box for a specific cluster. The left picture shows the original cluster in dark grey and all potential successors inside the black-bordered box in light grey: six clusters in this case. The black area in the middle of the box is the overlap, consisting of those pixels that are covered by both the original cluster and the successor. The black arrow shows the direction of the overall movement, which is 117°. On the right, the original cluster is shown together with the successor chosen by the algorithm. The direction of motion for this example is 108°. The distance between the two successive clusters is about 3 km, implying a velocity of about 10 ms^{-1}.

procedure. Merging occurs when, for two or more clusters in the radar data of $t = t_0$, the same successor is identified in the subsequent radar image. Splitting, where several successors arise from one cluster, is more difficult to identify. If all these successors overlap with the original cluster, then they will all be identified by the algorithm; but there are situations where it is difficult to identify all successors – for example, if one successor does not overlap with the original cluster while another successor does. In that case, only the cluster with the overlap will be chosen (see Appendix B).

Another problem is caused by clutter in the radar data, i.e. parts of the radar echo returned from ground without having any meteorological content. Several methods exist for automatic detection and elimination of clutter: for example, statistical techniques, the Doppler method, or a (static or dynamic) clutter map. The various methods are discussed in Meischner (2004), for instance. It is impossible to remove clutter completely without changing the meteorological information. In our case, the existence of the same clutter over a long time causes ambiguity in the tracking results. Two individual clusters that move over an area of permanent clutter at different times could misleadingly be assigned to the same cluster track, thus lengthening the time span of that track. Furthermore, clutter usually covers a small area with high values of reflectivity or precipitation rate. This increases the number of single cells, and so affects the statistics. The quantitative effect of clutter on our results has not been investigated here in detail, and is left for future research.

However, by tracking a cluster over time, we can determine its development. In this study, the cluster development within each time step is analysed, and a conceptual model of the cluster's life cycle is derived. The whole path of a cluster, from genesis, through all growth processes and interactions, until dissolving, is referred to as a 'track'. All clusters that are connected in any way, so that they are precursors or successors of each other, are assigned to the same track. Figure 10 shows an example of such a track. This cluster complex was tracked over a time span of 145 min. It starts as a single cell, passes through internal growth, merging, internal decay and splitting, and becomes a single cell again, before it finally dissolves. The maximum size of the track is 175 km^2, and the maximum number of individual cells is eight.

Altogether, we identified an average of 4900 tracks per day, ranging from 2400 to 9400. The mean length of the tracks is about 36 min, ranging from 29 min to 40 min for individual days. Splitting or merging occurred in 22% of all tracks.

4. Results

We have defined a cluster as being composed of individual cells, each of which is defined by a maximum in precipitation rate. Clusters with only one maximum are also referred to as single cells.

Both types of growth processes described in Section 1.3 can occur at the same time: clusters in their growth phase, for instance, show an increase not only in the number of embedded cells but also in the sizes of individual cells (see Figure 19). However, the key growth process we are considering here is the change in the cell number of a cluster: the number growth. A cluster with n maxima develops to a cluster with m maxima ($n \rightarrow m$, where $n, m \geq 0$) within a time step of 5 min. From general considerations, and also from the time sequence of radar images, we can define a typical life cycle of a cluster, as outlined in Section 1.3.

For any given 5 min time interval, each cluster can unambiguously and uniquely be assigned to one of the five basic life stages, so that the transitions from one stage to the next are also well-defined. Table II lists the percentages of these transitions. We differentiate here between two different approaches: the 'cluster-based' and 'transition-based' approaches.

- The cluster-based approach is shown in the upper part of the table. For each cluster identified in the radar data,

DOI: 10.1002/qj

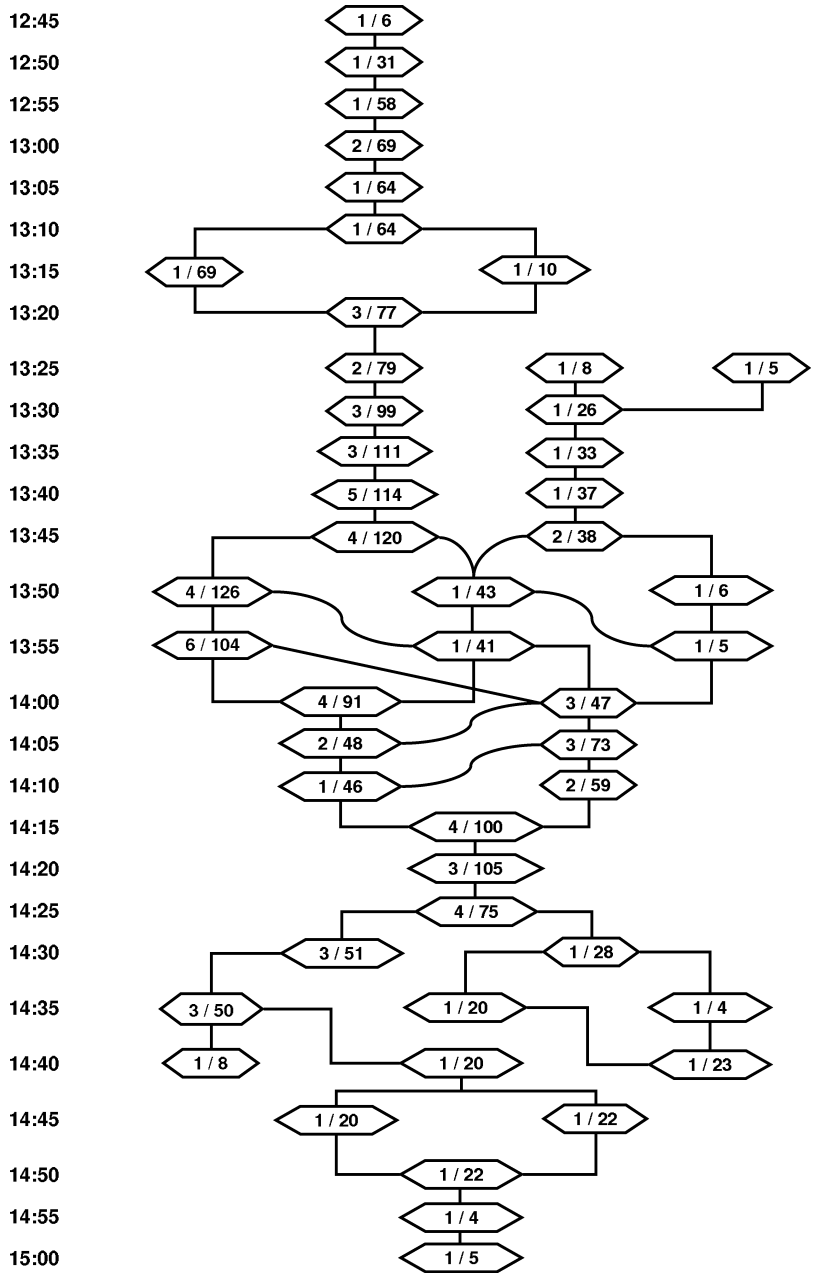

Figure 10. Example life cycle of a cluster track. Each box represents a cluster within the track, giving its cell number (left value) and cluster size in km^2 (right value). On the left of the figure is the time of day. The track has a life span of 145 min and a maximum size of 175 km^2.

Table II. Distribution of development stages, following the cluster-based and transition-based approaches. The numbers and percentages are associated with the various life stages and growth processes, from the total number of clusters and transitions respectively, counted for all 17 days. The difference between the cluster-based and transition-based approaches is explained in detail in the text.

	Total	Genesis	Growth	Stagnation	Decay	Dissolving
Clusters	1 151 257	(291 173)	330 334	400 280	183 068	237 575
	100%	(25%)	28%	35%	16%	21%
Transitions	1 571 849	291 173	263 726	529 521	249 854	237 575
	100%	18%	17%	34%	16%	15%

DOI: 10.1002/qj

the transition within the next time step is considered, so that we count one transition process per cluster. Each splitting thus counts as only one process, whereas merging counts as at least two processes, one for each cluster. Genesis is considered as an additional process. Therefore, the sum of the percentages is only 100% if genesis is omitted. Growth is composed of internal growth (80 000) and merging (250 000), and decay is composed of internal decrease (82 000) and splitting (102 000). A splitting, counted as one process, leads to an average of 2.3 new clusters.

- The transition-based approach is shown in the lower part of the table. For each transition $n \rightarrow m$, one process is counted. There is no discrimination between internal growth and merging, or between internal decrease and splitting. Each transition from the initial cluster n to any successor m is counted individually. Genesis ($n = 0$) and dissolving ($m = 0$) are also counted as transition processes.

Overall, in both approaches, the most common type of transition is stagnation, followed by genesis. In the transition-based approach, genesis, growth, decay and dissolving occur with similar frequencies; while in the cluster-based approach, decay and dissolving occur less frequently than genesis and growth. This is obviously due to the fact that in the cluster-based approach just one transition process is counted for splitting, while merging contributes one transition process for each cluster involved.

In what follows, we will often consider frequency distributions of clusters as a function of cell number p. Here, we always use relative frequencies, which are normalized by the total number of clusters identified in the radar data. We will show that these distributions can be well fitted by a power law:

$$N(p) = ap^b. \tag{1}$$

We follow Theusner (2007), who found that the frequency distribution of clusters as a function of cell number (see Figure 14) can be fitted by a power law on a wide range of time scales: for every hour of a day, for the mean of a day, or for a dataset of 39 days.

The slope b of the regression is always negative. Single cells, therefore, are always the most frequent clusters. The absolute value of b indicates the relationship between smaller and larger clusters. A large absolute value for the slope means a predominance of smaller clusters, while a smaller value indicates a lesser relative importance of small clusters.

The parameters a and b of the distribution were found by Theusner (2007) to vary from day to day, but remain constant over the course of a day. This implies that, on average, the frequency distribution remains self-similar, irrespective of whether the total number of clusters N_{abs} is increasing or decreasing. The total number of cells N_{total} at a given time t is calculated as:

$$\begin{aligned} N_{\text{total}}(t) &= \sum_{p=1}^{p_{\max}} N_{\text{abs}}(t) \cdot pN(p) \\ &= N_{\text{abs}}(t) \sum_{p=1}^{p_{\max}} pap^b. \end{aligned} \tag{2}$$

This result of Theusner (2007) imposes a constraint on the growth and decay processes, as growth and decay have to occur in such a way that the frequency distribution remains self-similar. The details of these processes, as depicted in Figure 4, are thus constrained.

In the following, we discuss the various life stages, and explain the growth and decay processes in more detail. For an illustration of these processes, see Figure 4.

4.1. Life stages

4.1.1. Genesis ($n = 0$)

About 25% of all clusters that can be identified in the radar data are found to be newly developed. This means, by definition, that they could not be identified as a successor of any already existing cluster.

Looking at the frequency distribution of newly-developed clusters as a function of cell number p in Figure 11, we see that about 96% of all newly-developed clusters are single cells. Clusters with two or three maxima may also be newly developed; but those with more than three maxima are unlikely to have appeared within a 5 min time step, and are probably clusters that were not detected previously because of technical problems.

The frequency distribution of newly-developed clusters is described by a power law (Equation (1)). The parameters a_{n} and b_{n} are determined by regression (relative frequencies smaller than $5 \cdot 10^{-4}$ being omitted for reasons of statistical sampling). Their values are given in Table III. The slope value $b_{\text{n}} = -4.69$ indicates the dominance of very small clusters, especially single cells,

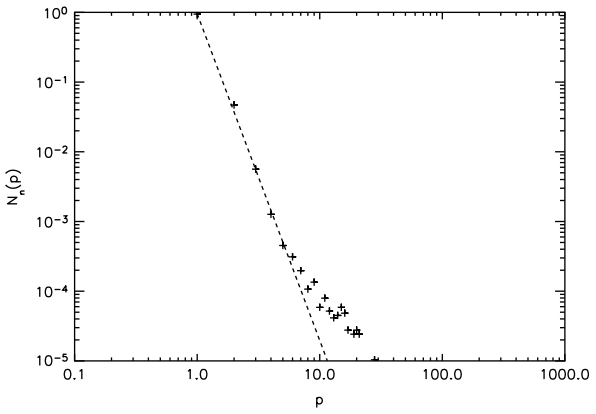

Figure 11. Average frequency distribution of newly-developed clusters $N_{\text{n}}(p)$, where p is the number of precipitation maxima (cells). Data with $N_{\text{n}}(p) > 5 \cdot 10^{-4}$ are fitted to a power law (Equation (1)). The distribution parameters a_{n} and b_{n} are given in Table III.

DOI: 10.1002/qj

resulting from the genesis process. The parameter a_n is the normalization constant, determined by the requirement that the distribution $N(p)$ sum to one. It represents the proportion of single cells, in this case 96%. Overall, new clusters are generated mainly as single cells.

4.1.2. Growth ($m > n$)

Cluster growth is defined as an increase in the number of cells within the cluster. This may be caused by two distinct growth processes.

- Internal growth occurs in about 24% of all growth cases (in the cluster-based approach). A new cell (or equivalently a new precipitation maximum) emerges within a cluster.
- Merging with neighbouring clusters occurs in about 76% of all growth cases (in the cluster-based approach). Figure 4 illustrates the merging process ('M'). Here, a six-cell and a three-cell cluster combine to form a ten-cell cluster. Merging may occur for various reasons (see Section 1). For example, it may simply be caused by areal growth of two nearby clusters, with subsequent attachment. According to Westcott (1994), such horizontal expansion is the most common way of merging. Another possibility is the generation of a new single cell between two clusters, forming a bridge. Clusters may also move towards each other. Our study does not distinguish between these merging processes.

Table III. Regression parameters: fits of frequency distributions to Equation (1), averaged over all 17 days. For the regression of the life span distribution (last row), p was replaced by life span d in Equation 1. Only data with $N > 5 \cdot 10^{-4}$ are used.

	Index	a	b
Genesis	n	0.96	−4.69
Dissolving	d	0.95	−4.61
Stagnation	s	0.81	−2.85
All clusters	v	0.69	−2.24
Life span	l	3.94	−2.28

Figure 12 shows the growth and decay of clusters for two different end products: $m = 1$ and $m = 7$. The bar labelled n represents the number of clusters with n cells that develop into an m-cell cluster. Dark bars illustrate the growth process ($m > n$), while light bars represent decay ($m < n$). Genesis ($n = 0$) and dissolving ($m = 0$) are not shown.

The growth process is illustrated in Figure 12(b). The dark bars from $n = 1$ to $n = 6$ indicate the number of smaller clusters that develop to a seven-cell cluster within one time step. It is clear that seven-cell clusters grow most commonly from single cells ($n = 1$), and next most commonly from six-cell clusters ($n = m - 1$). This pattern is followed for all cluster sizes m, as can be seen from the transition matrix (Figure 20, Section 4.4), which shows all transitions $n \rightarrow m$. The most common type of growth by merging is an increase by one cell. This is probably because most of the clusters are single cells. When a single cell merges with another cluster, the latter will increase by one cell. The single cell will grow by more than one cell, but if we always take the larger cluster as the reference we find a preference for one-cell increase. For internal growth, an increase by one or two cells inside a cluster is most likely within the short 5 min time step.

4.1.3. Stagnation ($m = n$)

Stagnation means that the number of cells p within a cluster stays constant within the 5 min time step. Nevertheless, the area of the cluster may change, or there may be an increase or decrease by one cell that is reversed within the time step. The algorithm cannot distinguish these possibilities. Stagnation ('St') is illustrated in Figure 4. About 35% of all clusters identified in the radar images stagnate; the remaining 65% change their size within the 5 min time interval.

More than 50% of all single cells remain single in the course of one time step, as can be seen in Figure 13. In contrast, just 10% of all 15-cell clusters stagnate within this time step. Interestingly, 65% of all tracked rain areas are single cells that remain single for their whole life.

Figure 14 shows that the frequency distribution of stagnating clusters is, as may be expected, dominated by single cells. Approximately 81% of all stagnating clusters

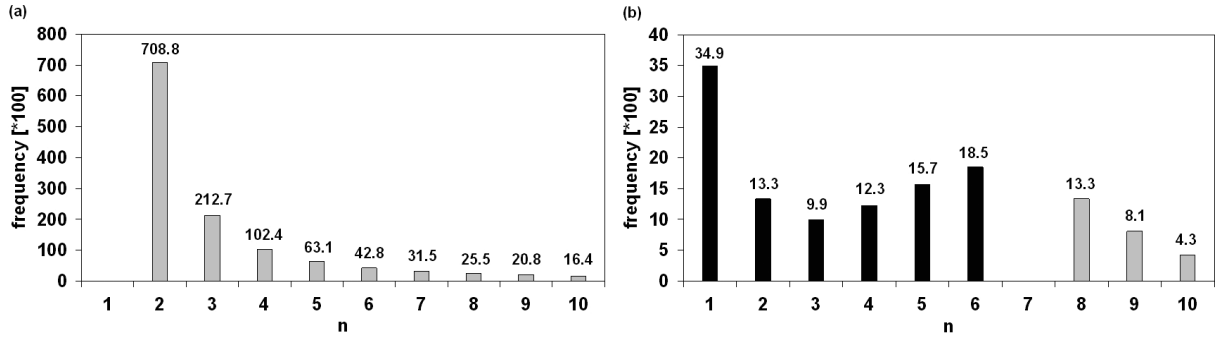

Figure 12. Transition distributions for clusters of size (a) $m = 1$ and (b) $m = 7$. The bar labelled n indicates the total number of transitions of a cluster of size n to one of size m. Dark bars represent the growth process ($m > n$), while light bars show decay ($m < n$). A summary of all the transitions can be found in Figure 20 (Section 4.4).

DOI: 10.1002/qj

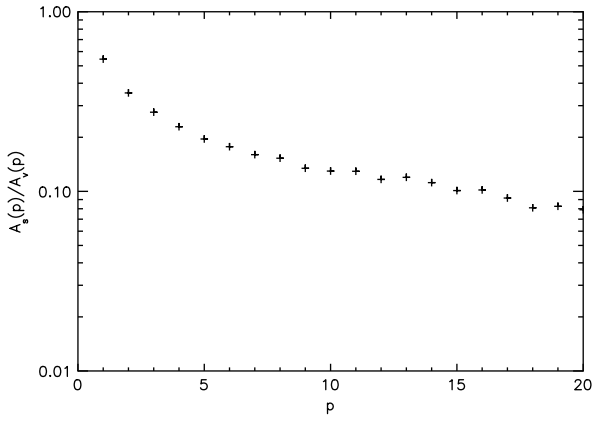

Figure 13. Ratio of the number of stagnating clusters A_s with p maxima to the total number of clusters A_v with the same cell number p. This ratio shows the proportion of all clusters with a specific cell number p that is stagnating within a time step of 5 min.

are single cells. This doubly-logarithmic presentation of the frequency distribution of stagnating clusters reveals a power law again (Equation (1)), with $b_s = -2.85$. The frequency distribution of all clusters yields, similarly, $b_v = -2.24$ (see Table III).

We now consider the number of larger clusters in relation to the number of smaller clusters, i.e. integrals over the respective frequency distributions from 6 to 50 for the larger ones and from 1 to 5 for the smaller ones. This ratio is smaller if only stagnating clusters are considered (0.018) than if all clusters are considered (0.067), and is larger if only non-stagnating clusters are considered (0.113). In this sense, larger clusters tend to change more frequently than smaller ones.

4.1.4. *Decay ($m < n$)*

Decay is defined as a cluster losing one or more maxima within a time step. Two types of decay processes may occur.

- One or more single cells or smaller clusters may split off within the given time interval of 5 min. This accounts for 55.5% of all decay cases (cluster-based approach). Figure 4 shows an example of a cluster with three maxima splitting into two smaller ones ('Sp'): a two-cell cluster and a single cell.
- There may be an internal decrease or disappearance of a cell inside a cluster. This accounts for 44.5% of all decay cases (cluster-based approach).

The decay process usually transforms a cluster with n maxima to a single cell and a cluster with $m = n - 1$ maxima. This is illustrated in Figure 12 for the two cases of $m = 1$ and $m = 7$ (light bars). The results for other values of m can be found in the transition matrix (Figure 20). Of all values of n greater than m, the value $n = m + 1$ represents the most frequent precursor. This implies that products of decay are predominantly generated from clusters with one cell more. The resulting distribution of decaying clusters (see Figure 14), showing a decrease with increasing cell number, also reflects the frequency distribution of all clusters.

4.1.5. *Dissolving ($m = 0$)*

The final disappearance of a cluster ('dissolving') is a decrease such that after 5 min the cluster no longer exists. Obviously, this is most likely to happen for small clusters and single cells. In fact, 95% of all clusters that disappear within one time step are single cells. Figure 15 shows the frequency distribution of disappearing clusters. The high absolute value of the slope ($b_d = -4.61$) indicates the dominance of single cells. There are some cases of larger clusters with more than three, and up to 50, maxima disappearing. However, such extreme cases are probably due to a temporary breakdown of a radar station, as the complete disappearance of a large cluster within 5 min does not seem realistic (see Figure 16).

4.1.6. *Summary*

In summary, the Lagrangian study of post-frontal shower cells and their life cycle reveals a typical structure.

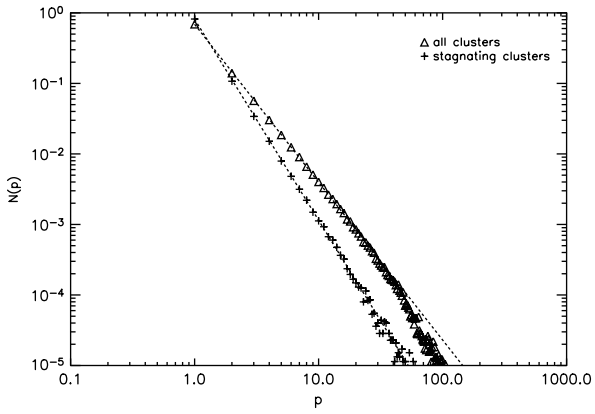

Figure 14. Average frequency distribution $N(p)$ of all clusters, and of stagnating clusters. Data with $N(p) > 5 \cdot 10^{-4}$ are fitted to a power law (Equation (1)). The distribution parameters a_s and b_s for the stagnating clusters, and a_v and b_v for all clusters, are given in Table III.

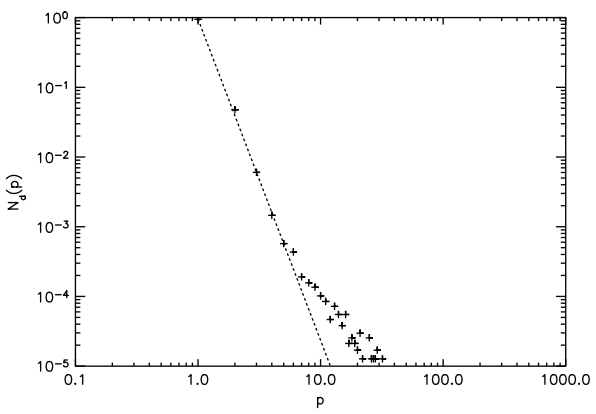

Figure 15. Average frequency distribution of all clusters without successor (disappearing clusters), as a function of the number p of maxima. Data with $N_d(p) > 5 \cdot 10^{-4}$ are fitted to a power law (Equation (1)). The parameters a_d and b_d are given in Table III.

DOI: 10.1002/qj

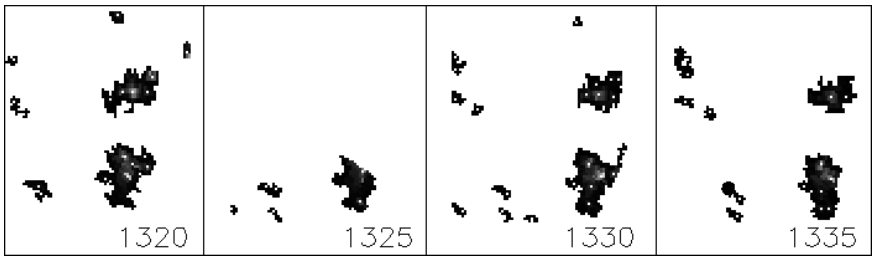

Figure 16. Time sequence showing gaps in the radar data. The temporary breakdown of a radar station and shadowing effects may lead to apparent sudden genesis or disappearance of large clusters.

Convective clusters emerge predominantly as single cells, and grow by gaining one cell after another or by merging with other clusters. Growth is interrupted by a phase of stagnation, followed by further growth or decay. This decay may take place by the loss of one cell after another or by splitting into two or more smaller clusters. Before a cluster disappears, it usually becomes a single cell; occasionally a cluster with two or three maxima disappears. Larger disappearing clusters are unlikely, and are interpreted as a consequence of data problems. This view may be simplified further by assuming that model clusters always change their cell numbers by one. This basic growth model is illustrated in Figure 21.

4.2. Life span

The life span of a cluster is defined as the time from genesis, through all growth processes, until the dissolving of the cluster. Because of the various interactions, the life span is not a function of a specific cluster, but rather of a set of clusters that are successors or precursors of each other (a track). A cluster has to be tracked at least once to be classified as part of a track. The minimum life span of a track is 15 min, as each transition process is assigned to a 5 min interval. About 10% of all clusters have neither precursor nor successor; these cannot be tracked, and thus have a life span of just 10 min. The frequency distribution of the life span of a cluster track thus defined can again be fitted to a power law (Figure 17). The coefficients of the regression are listed in Table III. The absolute value of the parameter $b_l = -2.28$, which is the slope of the doubly-logarithmic representation, indicates that short life spans predominate; but this is less than the corresponding parameter for the frequency distribution of newly-developed clusters ($b_n = -4.69$). About 80% of the tracks have a life span of 15–35 min.

4.3. The role of single cells

According to the frequency distribution (Figure 14), single cells represent the main fraction of clusters. In terms of covered area, however, they play only a minor role. This difference is illustrated in Figure 18. Single cells clearly dominate in number (about 69% of all clusters are single cells), but account for less than 15% of the total rain area. Furthermore, the decrease in frequency with increasing cell number p is very large compared

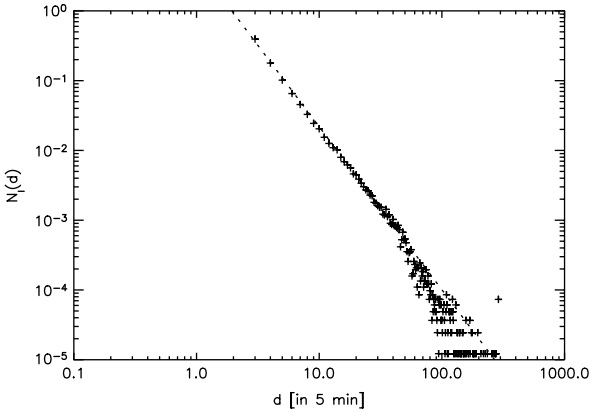

Figure 17. Average frequency distribution of the life span d of all clusters. Data with $N_l(d) > 5 \cdot 10^{-4}$ are fitted to a power law (Equation (1), with p replaced by life span d). The distribution parameters a_l and b_l are given in Table III.

to that of the covered area. Thus, larger cells dominate with respect to the covered area, although they occur rather seldom. This result reflects the fact that the area covered by a cluster increases with cell number, which is also shown in Figure 19. The mean area per cell is about 30 km^2.

4.4. Transition matrix

The characteristics described in Section 4.1 can be encapsulated in a single transition matrix. The number of clusters with n maxima that develop into a cluster with m maxima is determined for every possible combination ($n \rightarrow m$). The information is displayed in a two-dimensional array, the transition matrix, of size $n_{max} \times n_{max}$, where n_{max} is the maximum number of cells taken into account. An example of such a matrix is given in Figure 20, which displays data for all 17 days. For reasons of simplicity, the number of cells is limited to $n_{max} = 10$. In Figure 20(a), the total number of transitions from n to m maxima is shown in hundreds. For each splitting event, the transition from the original cluster to each successor is calculated as one event. Thus, the process of splitting into two parts yields two counts for the transitions. The same is true of merging: all transitions from a cluster to a successor are counted, even if the successor has an additional precursor. This means, for example, that if a cluster splits into three smaller clusters,

DOI: 10.1002/qj

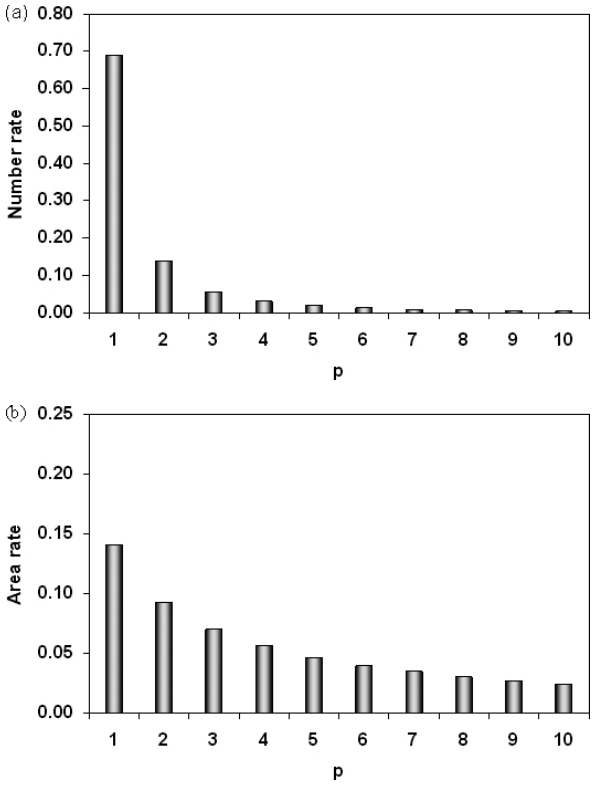

Figure 18. (a) Frequency distribution of clusters with cell number p (same data as Figure 14, but linear presentation). (b) Area covered by clusters with cell number p divided by the total precipitation area. Both figures display data for all 17 days.

we count three transitions; and if two clusters combine we count two transitions.

The diagonal entries shaded in dark grey represent the clusters that do not change their cell number within a time step (stagnation). All elements above this line represent decaying clusters ($m < n$); all elements below it represent growing clusters ($m > n$). Both above the diagonal and below it, the highest values are shaded in light grey. In the growth part, the highest values can always be found in the transition from n to $m = n + 1$. In the decaying part, the picture is more variable: clusters of all sizes develop predominantly to single cells ($m = 1$), while the second most likely transition is from n to $m = n - 1$. The more maxima a cluster contains, the more variable the decay. Besides the maximum value at $m = 1$, there are similar numbers of transitions to all smaller clusters.

As stated above, the results from Section 4.1 can be found again within the transition matrix. The diagrams in Figure 12 display, for example, two of the the rows of the matrix (a), with the first value and that of the diagonal omitted.

The development is rather complex, and the matrix has notable asymmetries. For example, a two-cell cluster can combine with a three-cell cluster to form a five-cell cluster or even a larger cluster in combination with internal growth. A five-cell cluster may also form from the combination of single cells with a larger cluster. Thus,

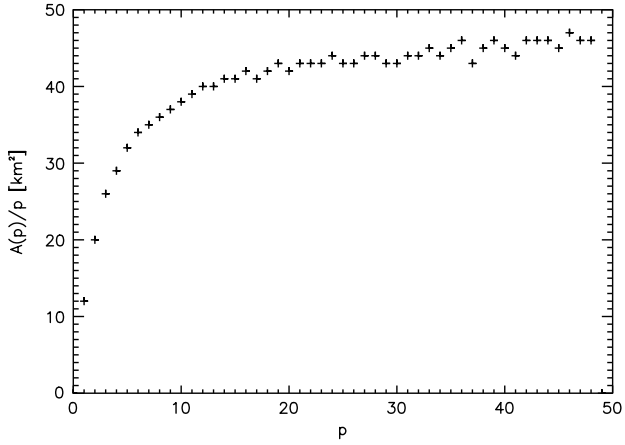

Figure 19. Mean area per cell as a function of the number p of enclosed cells. The area per cell increases strongly with p up to a cell number of about 10, and then converges to a value of about 45 km^2. The mean area per cell is 30 km^2.

the numbers of transitions $2 \rightarrow 5$ and $3 \rightarrow 5$ will not necessarily be the same.

Figure 20(b) shows the same field but normalized by the total number of n-cell clusters involved in a transition (equivalent to the column sum in matrix (a)). From this matrix, the frequencies of specific transitions of n-cell clusters to m-cell clusters can be read. Again, the diagonal represents stagnation, and is shaded in dark grey. Growth (below the diagonal) and decay (above the diagonal) show asymmetry: growth appears to be less likely than decay. One explanation for this is the method of normalization: the frequencies are related to the number of transitions starting from an n-cell cluster. In a splitting process, several smaller clusters emanate from one starting cluster, resulting in several transitions $n \rightarrow m_i$ with $n > m_i$. In contrast, merging results in only one transition at a time for a starting cluster: for each n_i-cell cluster contributing to the end m-cell cluster, one transition $n_i \rightarrow m$ with $n_i < m$ is counted. Although splitting and merging may have the same number of transitions, their frequencies in relation to the starting number n are different.

5. Conclusions

In this study we have used the new radar product of the DWD national radar network, the RZ-composite with 5 min resolution, to study the life cycle of post-frontal shower clouds. Interesting results concerning the geometrical nature of such clouds and their clusters were derived by Theusner (2007); however, those studies were based on an older radar product with a resolution of only 15 min, which necessitated the use of an Eulerian framework to study the shower fields. The RZ-composite allows the tracking of individual shower clouds in a Lagrangian framework. For this purpose, a tracking algorithm has been developed and used to study individual life cycles (tracks). This new algorithm is specifically adapted to the RZ-composite and the characteristics of

DOI: 10.1002/qj

(a)

m \ n	0	1	2	3	4	5	6	7	8	9	10
0	0.0	2239.1	113.3	14.4	3.5	1.4	1.1	0.5	0.4	0.3	0.3
1	2749.1	4329.5	708.8	212.7	102.4	63.1	42.8	31.5	25.5	20.8	16.4
2	137.0	790.9	567.8	204.0	75.5	36.1	19.4	12.8	9.1	7.2	5.4
3	16.5	244.7	209.4	180.0	88.4	38.7	18.7	10.4	6.7	4.4	3.7
4	3.7	114.5	75.4	91.1	79.8	48.6	23.3	12.9	6.0	4.1	2.7
5	1.3	67.7	34.9	40.1	48.4	41.8	28.3	15.1	8.1	4.5	2.9
6	1.0	45.3	18.6	18.1	24.5	28.2	25.4	18.6	10.0	6.3	3.5
7	0.6	34.9	13.3	9.9	12.3	15.7	18.5	16.7	13.3	8.1	4.3
8	0.4	25.5	8.3	6.2	6.0	8.4	11.1	12.7	11.6	9.1	5.8
9	0.4	20.6	6.8	4.5	4.0	4.6	5.9	7.7	8.8	7.9	6.8
10	0.2	17.1	5.2	3.4	2.8	2.7	3.4	4.9	5.8	6.4	6.0

(b)

m \ n	0	1	2	3	4	5	6	7	8	9	10
0	0.00	27.59	6.25	1.77	0.75	0.46	0,51	0.31	0.33	0.36	0.35
1	94.41	53.35	39.09	26.25	22.04	20.88	20.43	20.16	21.54	22.03	21.71
2	4.71	9.75	31.32	25.17	16.24	11.92	9.28	8.17	7.67	7.58	7.11
3	0.57	3.02	11.55	22.21	19.01	12.80	8.95	6.69	5.67	4.64	4.87
4	0.13	1.41	4.16	11.24	17.16	16.06	11.11	8.24	5.04	4.36	3.55
5	0.05	0.84	1.92	4.95	10.41	13.83	13.50	9.71	6.85	4.71	3.81
6	0.03	0.56	1.03	2.24	5.27	9.33	12.13	11.89	8.40	6.71	4.61
7	0.02	0.43	0.74	1.23	2.64	5.18	8.83	10.67	11.26	8.57	5.64
8	0.01	0.32	0.46	0.77	1.29	2.78	5.32	8.12	9.82	9.62	7.70
9	0.01	0.25	0.37	0.56	0.87	1.51	2.80	4.92	7.39	8.32	9.02
10	0.01	0.21	0.29	0.42	0.60	0.89	1.62	3.17	4.89	6.81	7.97

Figure 20. Transition matrix for all 17 days: (a) absolute numbers of transitions $n \rightarrow m$ (in hundreds); (b) the same matrix normalized by the total number of n-cell clusters involved in a transition.

mid-latitude shower clouds. In a first step, various characteristics of the cluster are determined; then, in a second step, the new position of the cluster is determined, for instance by means of the overall propagation direction. This is achieved by a correlation analysis of the complete post-frontal area. Over 17 days with post-frontal shower precipitation, almost 83 000 tracks can be identified, with a mean life span of about 36 min. From an analysis of all those tracks, we have defined the various stages of the life cycle, and determined the proportions of the various transitions between them. A typical life cycle comprises genesis, growth, stagnation, decay, and dissolving.

For all stages except growth and decay, the frequency distributions have been determined, and are found to fit well to a power law of the type $N(p) = ap^b$. The same distribution is found for the life spans of the tracks and the cell numbers of the clusters. Deviations typically occur for low frequencies because of limitations of the sample statistics.

One of the main implications of a power law is scale invariance. Power laws characterize a huge number of natural patterns, for example in physics, computer science, economics, finance, biology and the social sciences (Newman, 2005). Various theories have been proposed to explain the underlying processes. The observed growth mechanism of shower cells, as deduced from the transition matrix, fits the general properties of a Yule process. The key feature of this process is that entities increase their value (here the number of enclosed cells) at each

DOI: 10.1002/qj

time step with a certain probability in proportion to the value itself (Concas *et al.*, 2006). Physically we may explain the growth by the cell dynamics, which show updraughts that favour neighbouring growing cells but suppress those further away. In the case of the shower clouds, this implies that new shower cells grow preferably in the vicinity of existing cells or within an already-existing cluster. Investigation of the underlying principles is beyond the scope of this paper.

Looking at the transition rates, for instance in Figure 20, one recognizes the dominant role of single cells. Not only are these the most frequent clusters, but they are also predominantly involved in merging and splitting. In essence, clusters of all sizes grow predominantly by one cell at a time, either by internal growth or by merging. This observation leads to the proposition of a simple conceptional model to summarize these findings. In the framework of this model, we assume that a new cluster forms first as a single cell. The model ignores the fact that within the 5 min time step clusters with more than one cell could form. Single cells then grow by the two processes of internal growth and merging, as mentioned above. Figure 21 illustrates this process.

Considering the growth process in general (not confined to increases by one cell), we see that in 22% of all tracks, merging or splitting occurs. Dixon and Wiener (1993) found that 12% of the thunderstorms in their analysis were involved in merging or splitting. Despite the differences between post-frontal shower precipitation, which is mostly a mid-level convection phenomenon, and deep convection, approximately the same percentage of merging and splitting occurs for the two convective phenomena. As a complementary result, we may note that in the majority of cases (78%) clusters grow only internally, through a new cell forming within the existing cluster boundaries. A growth period is typically followed by a period of stagnation, before the cluster grows further again or starts to decay. The decay of clusters reflects their growth, i.e. decay always occurs one cell at a time as well. This may happen if an updraught collapses and the corresponding cell disappears, or if the whole cluster weakens and one cell becomes separated from the main body of the cluster. Finally, a cluster is terminated if the last remaining cell disappears. Further studies need to be performed to focus on genesis and dissolving during the diurnal cycle.

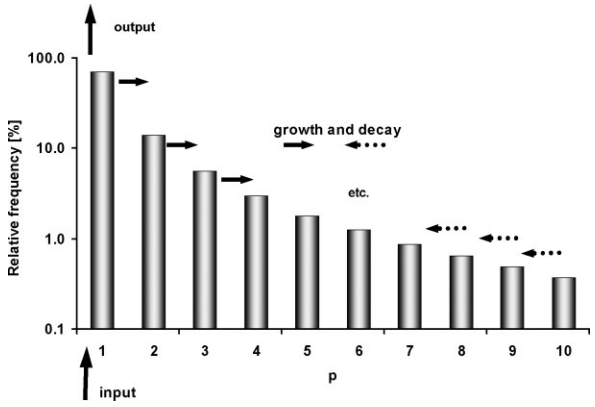

Figure 21. Elementary growth model of post-frontal convective clusters. The diagram shows the frequency of clusters as a function of cell number p. Clusters are generated predominantly as single cells. Growth and decay are effected by different processes, but preferentially proceed by one cell within a time step of 5 min. The dissolving of clusters also takes place through single cells.

This simple conceptual model covers most of the processes. In reality, however, growth and decay are much more complicated. Two results illustrate this. First, nearly all elements of the transition matrix (Figure 20) are non-zero, though the numbers may be small. Secondly, the case study of Figure 10 demonstrates this situation. More research is necessary in order for the growth and decay of larger clusters to be understood and quantitatively described.

Our studies deal with the specific synoptic situation of a post-frontal precipitation field, but cover a range of synoptic conditions. In the structural characteristics, this leads to a certain scatter in the parameters a and b of the observed power-law distribution (Theusner, 2007). Despite this variability, the situations investigated show the same overall structure and indicate the same convection regime. In another current study on the same topic, the focus is on the rain-rate characteristics and areal growth. Those analyses might lead to a further improvement in our understanding of the underlying processes.

Acknowledgements

The German Research Foundation (DFG) funded this work through its priority program 'Quantitative Precipitation Forecast' under grant number HA 1761/5-2. The RZ-composite used in this study was provided by the German Weather Service (DWD), which is kindly acknowledged.

A. Appendix: Sample from data file containing cluster characteristics

The various characteristics of each cluster are stored in hourly data files as described in Section 3. Table IV shows an example of the parameter list for 24 September 2004, 1000 UTC. The different columns represent the different parameters, which are as follows: 0 – time; 1 – label; 2 – area; 3 – cell number; 4 – mean precipitation rate; 5 – total precipitation; 6 – maximum precipitation rate; 7 – x value; 8 – y value; 9 – number of the track; 18 – precursor; 19–21 – successors. Each row shows the parameters of a specific cluster. These examples are chosen as they show some interesting features of cluster development. The first cluster (1631) has a precursor, but no successor; thus it is an ending cluster. The next two examples (1636 and 1645) have the same precursor: they merged within the preceding time step. Cluster 1656 is newly developed: it has no precursor, but does have a successor. Cluster 1660 is also newly developed, but

DOI: 10.1002/qj

this one has no successor either, and thus has a life span of only 10 min. Cluster 1658 has a precursor and several successors: this means that the cluster, which is a relatively large one with 36 maxima, splits within one time step into several smaller clusters.

B. Appendix: Algorithm for identification of the most likely successor

Clusters are tracked by means of a search box, as described in Section 3. To identify the most likely successor out of all potential successors found within this box, the following algorithm is used.

Case 1 There is only one potential successor, A.
- If overlap exists, then A is a successor.
- If no overlap exists, then A is only a successor if $\Delta d(A) < 40^\circ$ and $\Delta r(A) < 12$ km.

Case 2 There are $n > 2$ potential successors $A_i (i = 1, \ldots, n)$.
- If overlap exists, then all A_i with an overlap are successors.
- If no overlap exists, then A_i is a successor if $\Delta d(A_i) < 20^\circ$ and $\Delta r(A_i) < 20$ km; or if more than one successor is identified in this way then the cluster with the least change in size $\Delta s(A_i)$ is selected.

Case 3 There is no potential successor.
- The cluster is terminated.

The main criterion is the overlap, followed by the difference in direction compared to the overall movement of the rain field $\Delta d(A) = |d(A) - d(rainfield)|$ and the distance $\Delta r(A) = |r(A) - r(actual)|$. The direction $d(A)$ is calculated with respect to the actual cluster, i.e. it is the direction from the actual cluster to the potential successor A. The change in size $\Delta s(A_i) = |\text{area}(A) - \text{area}(actual)|$ is also used as a criterion. The values for the limits were found through systematic tests with a test dataset. If none of these criteria is satisfied, the cluster has no successor, and is therefore an ending cluster.

References

Austin GL. 1985. Application of pattern-recognition and extrapolation techniques to forecasting. *ESA Journal* **9**: 147–155.

Austin GL, Bellon A. 1982. 'Very-short-range forecasting of precipitation by the objective extrapolation of radar and satellite data'. Pp. 177–190 in *Nowcasting*, Browning KA (ed). Academic Press: London.

Bartels M, Weigl E, Reich T, Lang P, Wagner A, Kohler O, Gerlach N. 2004. Projekt RADOLAN – Routineverfahren zur Online-Aneichung der Radarniederschlagsdaten mit Hilfe von automatischen Bodenniederschlagsstationen (Ombrometer). Technical Report. Abschlussbericht. Deutscher Wetterdienst. Offenbach.

Bluestein HB. 1993. *Synoptic-Dynamic Meteorology in Midlatitudes*, Volume II. Oxford University Press: New York.

Bluestein HB. 1999. A history of severe-storm-intercept field programs. *Weather and Forecasting* **14**: 558–577.

Bluestein HB, McCaul EW, Byrd GP, Walko RL, Davies-Jones R. 1990. An observational study of splitting convective clouds. *Mon. Weather Rev.* **118**: 1359–1370.

Braham RR. 1996. The thunderstorm project. *Bull. Am. Meteorol. Soc.* **77**(8): 1835–1845.

Carvalho LMV, Jones C. 2001. A satellite method to identify structural properties of mesoscale convective systems based on the maximum spatial correlation tracking technique (MASCOTTE). *J. Appl. Meteorol.* **40**: 1683–1701.

Concas G, Marchesi M, Pinna S, Serra N. 2006. On the suitability of Yule process to stochastically model some properties of object-oriented systems. *Physica A* **370**(2): 817–831. DOI:10.1016/j.physa.2006.02.024.

Cunning JB, Holle RL, Gannon PT, Watson AI. 1982. Convective evolutions and merger in the FACE experimental area: mesoscale convection and boundary layer interactions. *J. Appl. Meteorol.* **21**: 953–977.

Dixon M, Wiener G. 1993. TITAN: Thunderstorm Identification, Tracking, Analysis, and Nowcasting – a radar-based methodology. *J. Atmos. Oceanic Technol.* **10**(6): 785–797.

Fu D, Guo X. 2006. A cloud-resolving study on the role of cumulus merger in MCS with heavy precipitation. *Adv. Atmos. Sci.* **23**(6): 857–868. DOI:10.1007/s00376-006-0857-9.

Jewett BF, Wilhelmson RB. 2006. The role of forcing in cell morphology and evolution within midlatutude squall lines. *Mon. Weather Rev.* **134**: 3714–3734.

Johnson JT, MacKeen PL, Witt A, DeWayne Mitchel E, Stumpf GJ, Eilts MD, Thomas KW. 1998. The cell storm identification and tracking algorithm: an enhanced WSR-88D algorithm. *Weather and Forecasting* **13**: 263–276.

Lang P, Plörer O, Munier H, Riedl J. 2003. KONRAD – Ein operationelles Verfahren zur Analyse von Gewitterzellen und deren Zugbahnen, basierend auf Wetterradarprodukten. *Berichte des Deutschen Wetterdienstes* 222. Technical Report. Deutscher Wetterdienst: Offenbach.

Lee BD, Jewett BF, Wilhelmson RB. 2006a. The 19 April Illinois tornado outbreak. Part I: Cell evolution and supercell isolation. *Weather and Forecasting* **21**: 433–448.

Lee BD, Jewett BF, Wilhelmson RB. 2006b. The 19 April Illinois tornado outbreak. Part II: Cell mergers and associated tornado incidence. *Weather and Forecasting* **21**: 449–464.

Li PW, Lai EST. 2004. Applications of radar-based nowcasting techniques for mesoscale weather forecasting in Hong Kong. *Meteorol. Appl.* **11**: 253–264. DOI:10.1017/S1350482704001331.

Meischner P. 2004. *Weather Radar*. Springer: Berlin, Heidelberg.

Mesnard F, Sauvageot H. 2003. Structural characteristics of rain fields. *J. Geophys. Res.* **108**(D13): 4385–4401.

Mueller C, Saxen T, Roberts R, Wilson J, Betancourt T, Dettling S, Oien N, Yee J. 2003. NCAR auto-nowcast system. *Weather and Forecasting* **18**: 545–561.

Newman MEJ. 2005. Power laws, Pareto distributions and Zipf's law. *Contemp. Phys.* **46**(5): 323–351. DOI:10.1080/00107510500052444.

Table IV. Sample from data file containing cluster characteristics. Different rows represent different clusters; different columns represent different characteristics. See text for explanation.

0	1	2	3	4	5	6	7	8	9	...	18	19	20	21
1015	1631	16	1	9	154	11	442	134	6024	...	1102	0	0	0
1015	1636	26	1	22	574	50	543	137	10734	...	1098	2127	2133	0
1015	1645	6	1	11	66	17	543	145	10734	...	1098	2144	0	0
1015	1656	4	1	10	40	11	640	157	6099	...	0	2157	0	0
1015	1658	1271	36	22	28888	96	556	184	10734	...	1123	2160	2161	2175
1015	1660	7	1	11	77	17	368	169	0	...	0	0	0	0

Pierce CE, Hardaker PJ, Collier CG, Haggett CM. 2000. GANDOLF: A system for generating automated nowcasts of convective precipitation. *Meteorol. Appl.* **7**: 341–360.

Pierce CE, Ebert E, Seed AW, Sleigh M, Collier CG, Fox NI, Donaldson N, Wilson JW, Roberts R, Mueller CK. 2004. The nowcasting of precipitation during Sydney 2000: an appraisal of the QPF algorithms. *Weather and Forecasting* **19**: 7–21.

Rinehart RE. 1981. A pattern-recognition technique for use with conventional weather radar to determine internal storm motions. *Atmos. Tech.* **13**: 119–134.

Rinehart RE, Garvey ET. 1978. Three-dimensional storm motion detection by conventional weather radar. *Nature* **273**: 287–289.

Tao WK, Simpson J. 1989. A further study of cumulus interactions and mergers: three-dimensional simulations with trajectory analysis. *J. Atmos. Sci.* **46**(19): 2974–3004.

Theusner M. 2007. *Structural Characteristics of Convective Rainfields*. Dissertation, Institut für Meteorologie und Klimatologie, Hannover.

Theusner M, Hauf T. 2004. A study on the small scale precipitation structure over Germany using the radar network of the German Weather Service. *Meteorol. Z.* **13**: 311–322. DOI:10.1127/0941-2948/2004/0013-0311.

Turpeinen O. 1982. Cloud interactions and merging on day 261 of GATE. *Mon. Weather Rev.* **110**: 1238–1254.

Tuttle JD, Foote GB. 1990. Determination of the boundary layer airflow from a single doppler radar. *J. Atmos. Oceanic Technol.* **7**: 218–232.

Westcott NE. 1984. A historical perspective on cloud mergers. *Bull. Am. Meteorol. Soc.* **65**(3): 219–226.

Westcott NE. 1994. Merging of convective clouds: cloud initiation, bridging, and subsequent growth. *Mon. Weather Rev.* **122**: 780–790.

Westcott NE, Kennedy PC. 1989. Cell development and merger in an Illinois thunderstorm observed by Doppler radar. *J. Atmos. Sci.* **49**(1): 117–131.

Weusthoff T. 2005. *Beiträge zur Entwicklung eines stochastischen Niederschlagsmodells zur Simulation postfrontaler Schauer*. *Diplomarbeit*, Institut für Meteorologie und Klimatologie, Hannover.

Wilson JW, Crook NA, Mueller CK, Sun J, Dixon M. 1998. Nowcasting thunderstorms: a status report. *Bull. Am. Meteorol. Soc.* **79**: 2079–2099.

Witt A, Johnson JT. 1993. 'An enhanced storm cell identification and tracking algorithm'. Pp. 514–521 in *26th Int. Conf. on Radar Meteorology*, Norman, OK. American Meteorological Society.